JOURNAL OF MATERIALS SCIENCE 12 (1977) 1879–1894

The structure of the γ' extended solid solution in a splat-cooled Ag-50 at.% Cu alloy

P.G. BOSWELL, G.A. CHADWICK
Department of Mining and Metallurgical Engineering, University of Queensland, St. Lucia, Brisbane, Australia.

The structure of the γ' extended solid solution in electron transparent areas of a splat-cooled Ag–50 at.% Cu alloys was examined by transmission electron microscopy. This phase was usually found to be spinodally decomposed at large grain sizes ($\simeq 1\ \mu m$ in diameter), in contrast to X-ray diffraction data indicating that the γ' solid solution was undecomposed. A solidification model for rapidly quenched eutectic alloys is proposed to account for the observed structure of the splat-cooled alloy. A transformation curve for the spinodal decomposition of γ' is also calculated and related to predictions derived from the solidification model.

1. Introduction

Duwez *et al.* [1,2] examined splat-cooled Ag–Cu alloys using X-ray methods and reported that rapid solidification gave a continuous series of metastable fcc solid solutions (designated γ') with a +1% lattice parameter deviation from the Vegard line. This experiment is often presented as a classic example of the production, by splat-quenching techniques, of a highly extended phase uncomplicated by extensive solid-state transformation or competing solidification reactions [3]. However, Stoering and Conrad [4] conducted a detailed electron metallographic examination of the structure of splat-cooled Ag–50 at.% Cu foils and they concluded that the γ' phase invariably decomposed during quenching: results reported by other investigators [5,6] appear to confirm this conclusion. Any fine-scale structure, of the type described by Stoering and Conrad [4], in the transformed γ' phase would probably not be detected by the X-ray methods used by Duwez *et al.* [1,2]. Hence it has not been demonstrated that a homogeneous untransformed γ' phase can be retained at room temperature by splat-cooling concentrated Ag–Cu alloys, despite the frequent supposition to the contrary.

Stoering and Conrad's [4] observations also suggested that the γ' phase transformed both by a nucleation and growth reaction and by spinodal decomposition, the latter evidently being favoured at the higher solid-state quenching rates obtained by cooling the quenching substrate with liquid nitrogen.

An electron metallographic investigation of the microstructures of a splat-cooled Ag–50 at.% Cu alloy was therefore undertaken with the view to ascertaining whether or not untransformed γ' could be retained at room temperature, and to obtaining positive evidence for the spinodal decomposition of γ'. It was also hoped that if spinodal decomposition occurred during quenching, then it would be possible to compare the observed characteristics of the transformed microstructures with theoretically predicted values of the same characteristics, thereby yielding estimates of solid-state cooling rates during splat-quenching. Moreover, efforts were made to calculate cooling rates at the solidification temperature by correlating as-solidified eutectic structures, observed in the splat-cooled foils, with similar structures formed under known conditions. Taken together, these calculated cooling rates in the solid and

liquid states should give some indications of the complete thermal histories of particular foil areas. Surprisingly, investigators have hitherto only concentrated on calculating splat-cooling rates at the solidification temperature from properties of as-solidified eutectic or dendritic [7] structures.

2. Experimental

Several foils of a high purity Ag–50 at.% Cu alloy were prepared by splat-cooling 200 mg charges of the molten alloy on to a liquid nitrogen cooled, copper substrate. A "gun" type quenching device [8], with the quenching chamber maintained at $\simeq 10^{-4}$ torr, was used. Examination of the foils by X-ray powder diffractometry and transmission electron microscopy was, in some cases, initiated within 10 to 20 min of splat-cooling. In other cases, the foils were allowed to age at room temperature in a vacuum of 10^{-5} torr prior to examination by the same methods. The X-ray data were obtained with monochromated $Cu_{K\alpha}$ radiation, pulse height analysis and a continuous scanning speed of 1/8 deg. min^{-1} and the electron metallographic observations of unthinned foils were made at 200 kV with a JEM200 STEM instrument.

3. Results and discussion

3.1. X-ray Diffractometry

Fig. 1 contains a typical X-ray diffractometer trace for an as-quenched Ag–50 at.% Cu foil over the 2θ angular diffraction range within which the (1 1 1) and (2 0 0) reflections of all the co-existing phases arose. In order to illustrate the presence of small volume fractions of several minor phases, a chart recorder full-scale deflection range that corresponded to 1/5 of the maximum signal was used. The proposed indexing of the various reflections are represented by vertical lines drawn using the calculated lattice parameters summarized in Table I. Wherever possible, these parameters were determined by means of a least-squares refinement of the diffraction data with 2θ angles greater than 90°. The trace demonstrates that the as-quenched foils were predominantly composed of the γ' phase ($a_0 = 0.3878 \pm 0.0003$ nm) with a strong (1 1 1) preferred orientation. The γ' peaks were broad, indicating that decomposition may have occurred, but diffraction intensity attributable to a precipitated phase or transformation structure could not be resolved. The second trace given in Fig. 1 was obtained after ageing the as-quenched foil at room temperature for four months and it is observed that the γ' phase had completely decomposed to the equilibrium α and β fcc solid solutions.

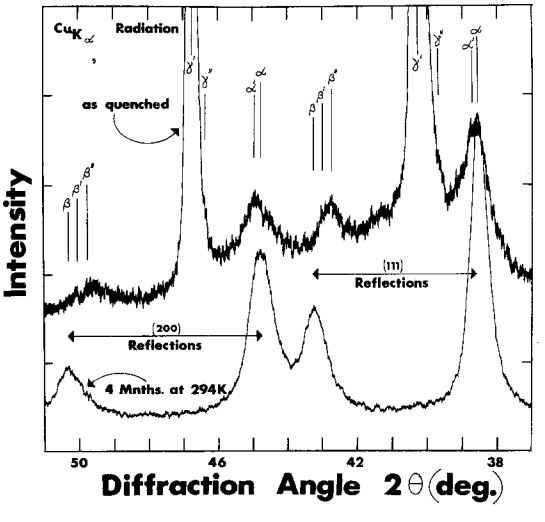

Figure 1 Typical X-ray diffractometer traces of a splat-cooled Ag–50 at.% Cu foil: upper trace, as quenched; lower trace, aged 4 months at room temperature. See Table I for lattice parameters of indexed phases.

The reflections corresponding to less supersaturated phases that also arose in the as-quenched foil were not particularly well defined, but they could be described in terms of α', β', γ' and γ'' phases (see Table I for lattice parameters). Fig. 1 shows that the α' and β' reflections remained at the end of the ageing treatment so the α' and β' phases are probably the consitutents of the discontinuous precipitation reaction that has been described by Stoering and Conrad [4]. The reflections indexed as arising from β'' and γ'' phases disappeared upon ageing, indicating that these two solid solutions may be related. Stoering and Conrad [4] noted the apparent absence of a Cu-rich phase in association with their γ'' phase, formed as a result of the partial decomposition of γ', and it is possible that β'' is the missing Cu-rich phase.

3.2. Transmission Electron microscopy

3.2.1. As-quenched foils

The grain size in electron-transparent regions of as-quenched foils was observed to vary over about three orders of magnitude, from $\simeq 3$ nm to $\simeq 2$ μm. This remarkably large variation implied that the phases present experienced a wide range of thermal histories and this inference was confirmed by

TABLE I Summary of f c c phases identified by X-ray diffraction in splat-cooled Ag–50 at. % Cu foils.

Phase	Lattice parameter (nm)			Occurrence (this study)		Description
	Observed	Reported	Reference	as-quenched	aged 4 months at 294 K	
γ'	0.3878 ± 0.0003	0.3876 ± 0.0003	[1, 2, 4, 6, 9]	√		1% deviation from Vegard's Law
γ''	0.3925 ± 0.0009	0.3953 ± 0.0006	[4, 6]	√		3% deviation; decomposed γ' [4] arises with β'' (?)
α	0.4051 ± 0.0007	0.4063 ± 0.0009	[6]		√	equilibrium Ag terminal solid solution
α'	0.4030 ± 0.0009	0.4030 ± 0.0010	[4, 5]	√	√	discontinuous reaction product [4, 6]; arises with β'
β	0.3628 ± 0.0003	0.3627 ± 0.0007	[6]		√	equilibrium Cu terminal solid solution
β'	0.3644 ± 0.0008	0.3653 ± 0.0008	[4, 5]	√	√	discontinuous reaction product [4, 6]; arises with α'.
β''	0.3679 ± 0.0008			√		possibly the missing Cu-rich phase arising with γ'' [4]

the observation of a variety of grain morphologies and microstructures. Generally speaking, the observed structures could be classified according to the grain size as follows: (a) coarse-grained material (grain diameter $\simeq 1\,\mu$m); (b) medium grain-sized material (grain diameter $\simeq 0.1$ to $0.01\,\mu$m); and (c) fine-grained material (grain diameter $\simeq 0.003\,\mu$m).

The coarse-grained material could be examined in detail and the only significant complication observed in microstructures of this type was that spherical eutectic cells were occasionally found to be embedded within the large-grained material. The morphological characteristics of the large grains and the eutectic cells will be discussed in Sections 3.2.1.1 and 3.2.1.2 respectively.

Material with an intermediate grain size was usually observed to be faulted or twinned or distorted to such a degree that it was impossible to identify the phases present and their morphologies. Detailed examinations of some of these complex structures were carried out but the results obtained will not be presented in this communication as they do not bear heavily upon the present discussion.

The very small grain size of the fine-grained material precluded a detailed investigation of its structure by transmission electron microscopy. However, two types of fine-grained material, distinguishable by their diffraction effects and imaging properties, were identified. These two structures were found to compise γ' and (possibly) γ'' phases, respectively, and Sections 3.2.1.3 and 3.2.1.4, deal with their morphological characteristics. Finally, β'', the remaining metastable phase detected by X-ray diffractometry, could not be located by transmission electron microscopy so the morphology of this phase was not investigated.

3.2.1.1. Coarse-grained material. Foil areas composed of large ($\simeq 1\,\mu$m diameter) grains were frequently located and BF* micrograph of a typical example is reproduced in Fig. 2a. It was noted that these large grains were often elongated (Fig. 2b) and that more equiaxed grain morphologies gave symmetric extinction contour patterns when the electron beam was exactly parallel to certain crystallographic directions (Fig. 2c). The former observation implied that a large heat flow

* BF = Bright field

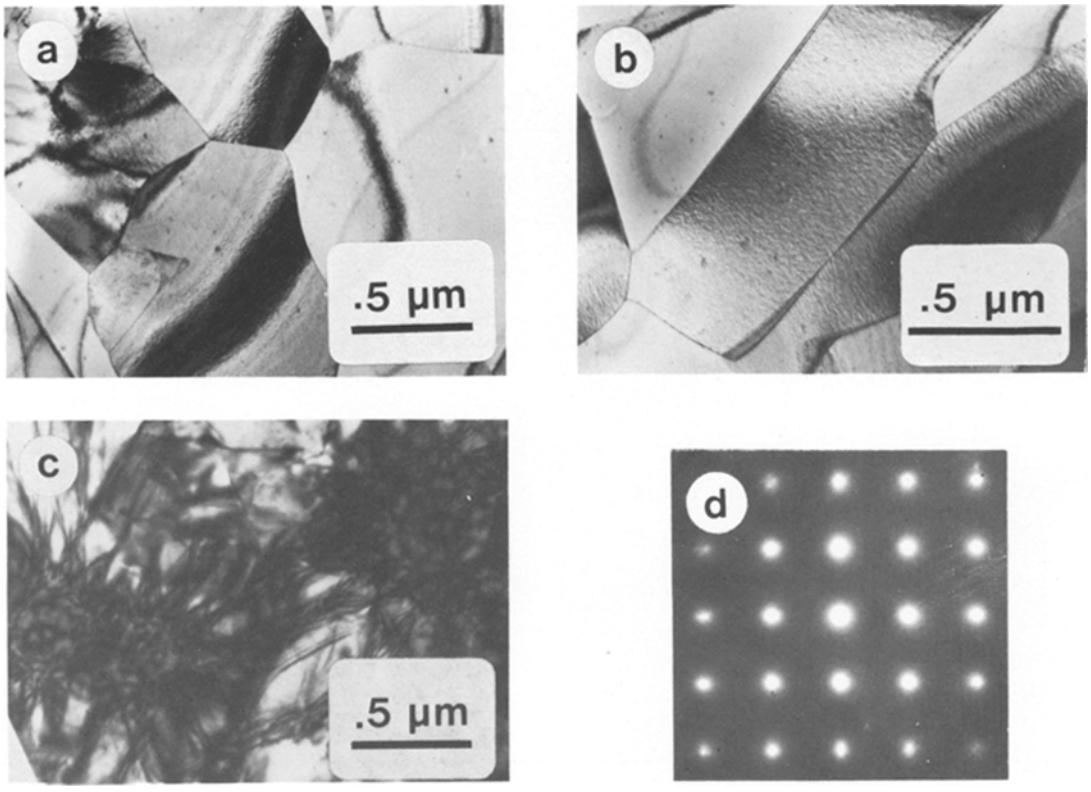

Figure 2 Coarse-grained material: BF micrographs of (a) typical grains, (b) elongated grains, (c) a lens or dome-shaped grains with symmetric extinction contour patterns (d) typical SADP, [1 0 0] zone axis, could be indexed in terms of γ' ($a_0 = 0.388 \pm 0.006$ nm).

component in the plane of the foil was established during the solidification of the large grains [10]. The latter observation indicated that roughly equiaxed grains were dome- or lens-shaped, due to radial solidification from a nucleation site located within the grains and either adjacent to a foil surface (for dome-shaped grains) or removed from the surface (for lens-shaped grains). All the single crystal SADPs* taken from the large grains, such as the pattern shown in Fig. 2d for a ⟨1 0 0⟩ zone axis, could be indexed in terms of the γ' phase with a lattice parameter of 0.388 ± 0.006 nm.

The γ' grains shown in Fig. 2 revealed weak mottling and their accompanying SADPs contained diffuse diffracted intensity around matrix reflections. A detailed investigation of the origins of these effects was undertaken. However, preliminary results indicated that a very thin epitaxial oxide layer had frequently formed on the surfaces of γ' grains during splat-cooling and this oxide was observed, on occasion, to mask the underlying γ' structure. The morphology of the oxide was dependent on the crystallography of the γ' free surface so in order to avoid confusion it was necessary to examine grains with surface normals that were parallel to specific γ' directions, and to the beam direction. Observations were made with ⟨1 0 0⟩, ⟨1 1 0⟩ and ⟨1 1 1⟩ zone axes parallel to the beam, but since adequate examples of the observed diffraction and imaging effects are provided by SADPs and micrographs taken in ⟨1 0 0⟩ orientations, examples corresponding to ⟨1 1 0⟩ and ⟨1 1 1⟩ orientations will not be presented. Furthermore, so as to prevent misinterpretation of the diffuse scattering effects, it was necessary to record diffraction patterns taken with precisely orientated γ' grains.

The dome- or lens-shaped grain morphology facilitated the tilting-up of exact crystal orientations because it was a simple matter to establish symmetric contour patterns within the γ' grains. In cases where the grains did not have convex surfaces it was necessary to obtain the required orientations by tilting the foil so as to equalize the

*SADP = Selected area diffraction pattern.

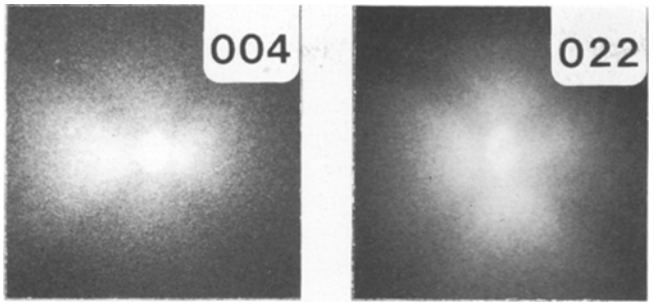

Figure 3 Enlargements of the (0 0 4) and (0 2 2) γ' reflections of Fig. 2d.

intensities of several high-order reflections that were symmetrically disposed about the transmitted beam. Unfortunately, the observed Kikuchi patterns were very weak and could not be used to establish exact orientations.

SADPs taken in $\langle 1\,0\,0\rangle_{\gamma'}$ orientations, as for example the pattern of Fig. 2d, revealed crosses of diffracted intensity centered on the transmitted beam and all the γ' reflections, with the arms of the crosses in cube directions. These crosses are shown more clearly in the enlargements (Fig. 3) of the (0 0 4) and (0 2 2) γ' reflections of the pattern provided in Fig. 2d: it can be seen that the crosses comprise triangular-shaped sidebands. The tilting procedures outlined above ensured that exact crystal orientations were established, so the sidebands did not correspond to the intersections of continuous rel-rods with a slightly misoriented reciprocal lattice section. There was a small asymmetry of the sideband intensity in a given cube direction due to the presence of the epitaxial oxide layer. In the case of a [1 0 0] zone axis, this layer was observed to produce regions of diffuse intensity on the low diffraction angle side of the γ' reflections. Identical diffraction effects have been reported to arise from thin epitaxial Cu_2O layers on the {2 0 0} surfaces of copper crystals [11]. These regions of weak intensity, combined with those produced by double diffraction, frequently modified the sideband intensities in the manner demonstrated by the enlargements of Fig. 3.

Fig. 4 gives BF and DF* micrographs of a large γ' grain with wide {0 0 2} type extinction contours running across the grain. Weak contrast striations in $\langle 1\,0\,0\rangle_{\gamma'}$ directions can be observed in dynamical regions near the contours. It was noted that the

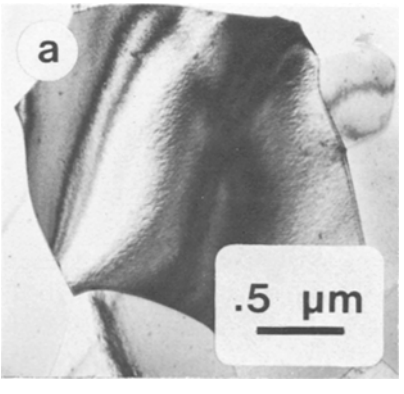

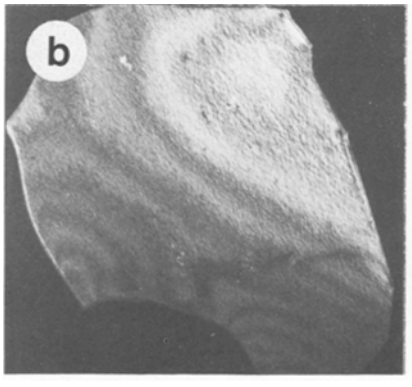

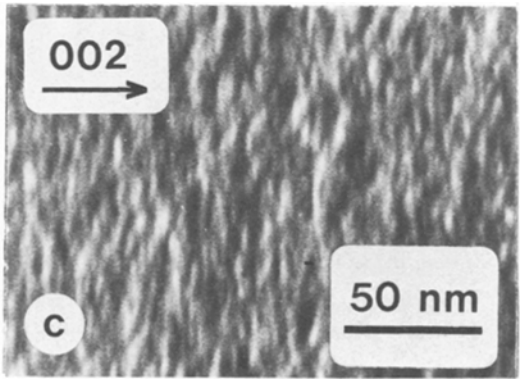

Figure 4 Partially decomposed γ' grain corresponding to the SADP of Figs. 2d and 3: (a) BF micrograph, (b) DF micrograph (both [1 0 0] γ' zone axis parallel to beam and foil normal), (c) enlargement of dynamical 2-beam area of (b), $\mathbf{g} = (0\,0\,2)$.

*DF = Dark Field.

high-resolution (tilted illumination) DF image revealed the striations over a larger area than the corresponding BF image and an enlargement of a dynamical region of the DF micrograph of Fig. 4b is reproduced in Fig. 4c: the zone axis is $\langle 1\,0\,0\rangle_{\gamma'}$, the reciprocal lattice vector of the operating reflection $\mathbf{g} = (0\,0\,2)$, and the striations are normal to $\mathbf{g}$. An orthogonally orientated set of striations arose in the same grain with $\mathbf{g} = (0\,2\,0)$ and the average striation spacing λ_{exp} for both sets was estimated to be 5.5 ± 1.5 nm.

While it is appreciated that fine scale microstructures developed as a result of nucleation and growth processes generally cannot be distinguished metallographically, or on the basis of electron diffraction patterns, from spinodally decomposed structures [12], nevertheless it is possible to examine whether or not the observed imaging and diffraction effects can be consistently interpreted in terms of the latter type of structure. The Fourier spectrum of a spinodally decomposed, compositionally modulated crystal has two components, namely a radial component describing the range of wavelengths and a tangential component describing the range of orientations of the modulations [13]. These two components could give rise to the crosses of diffuse intensity shown in Fig. 3 [12]. It will be assumed that the wavelength of the radial Fourier component receiving maximum amplification λ_m is equal to the wavelength λ_{calc} calculated using the Daniel–Lipson relation [14],

$$\lambda_{calc} = \frac{a_0 h \tan\theta}{\sqrt{(h^2 + k^2 + l^2)}\Delta\theta} \qquad (1)$$

where $\Delta\theta$ is the observed angular separation between the sidebands and the main $\{h\,k\,l\}$ reflection, θ is the diffraction angle of the main reflection, and a_0 is the lattice parameter of a cubic crystal. This expression gives an average calculated λ_{calc} of 5.0 ± 1.0 nm for several reflections of the SADP of Fig. 2d and an average λ_{calc} of 5.4 ± 1.2 nm for SADPs taken from five other striated γ' grains in different foils. The errors in the λ_{calc} values calculated from Equation 1 are considerably smaller than the errors in λ_{exp} wavelengths estimated from micrographs because the latter are subject to large microscope calibration errors and measurement errors [15].

Compositional modulations produced by spinodal decomposition frequently develop net matrix contrast in the elastically soft directions of the matrix ($\langle 1\,0\,0\rangle$ in the case of γ') [15]. Hence the observations, in BF and DF micrographs, of $\langle 1\,0\,0\rangle$ striations that are produced by strain contrast effects and which have average separation distances λ_{exp} approximately equal to λ_{calc} suggest that the γ' phase spinodally decomposed. Moreover, both λ_{exp} and λ_{calc} were found to be constant, within experimental error, throughout foils that had been splat-quenched to 150 K and examined after ageing at room temperature for 2×10^3 s, this being the total time required to mount the foils in the microscope and to subsequently locate a suitable area.

3.2.1.2. Eutectic cells. Occasionally, spherical eutectic cells, composed of radially diverging lamellae of the terminal α and β phases, were observed to be embedded within partially decomposed γ' grains identical to those described in the preceding Section. Fig. 5 shows typical examples of the cells and also demonstrates the tendency for the γ' grains surrounding the cells to be elongated in directions normal to the boundaries between the thin electron-transparent area and the adjacent thicker regions. The eutectic cells should not be confused with the discontinuous precipitation reaction products described by Stoering and Conrad [4] because the latter were reported to (a) nucleate at γ' grain boundaries, (b) consume γ' grains which had partially decomposed during splat-quenching to give Ag-rich clusters in a Cu-

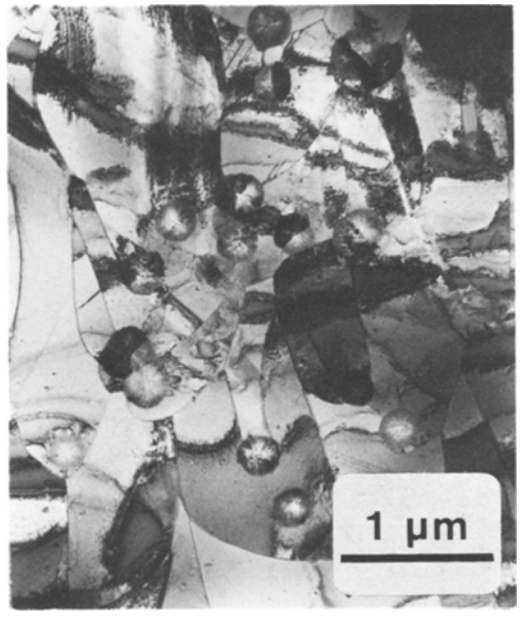

Figure 5 Eutectic cells embedded in partially decomposed γ' phase.

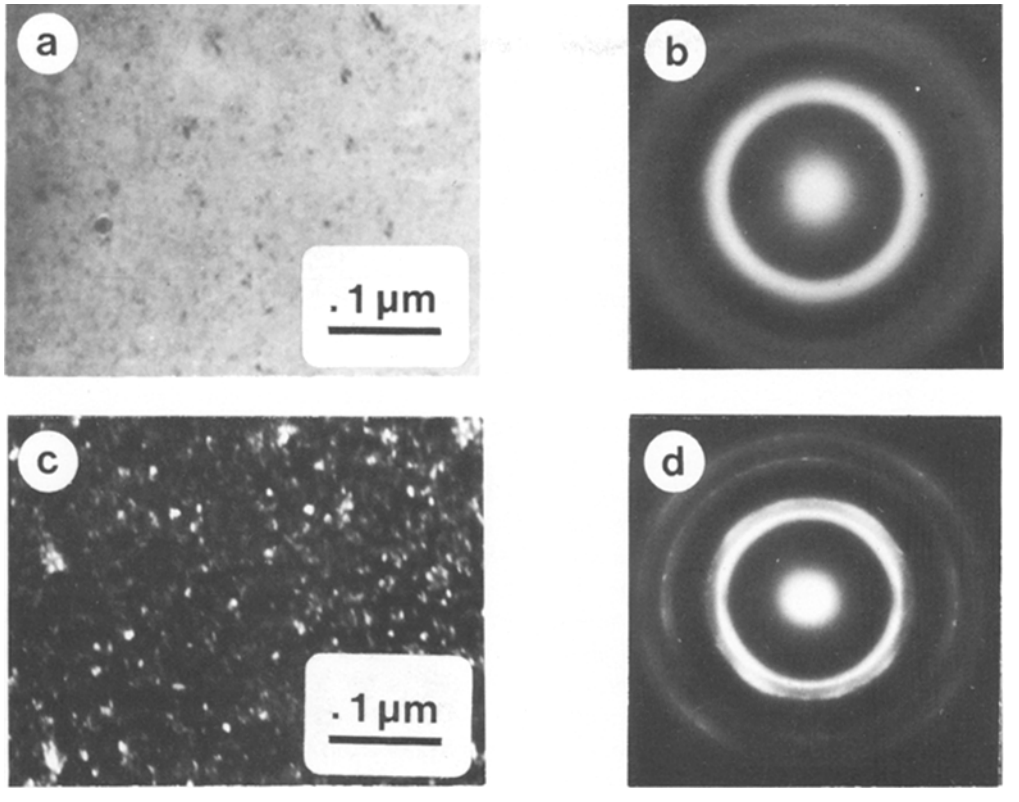

Figure 6 Fine-grained material; γ' phase: (a) BF micrograph, (b) SADP (c) DF micrograph, all with foil normal parallel to beam, (d) SADP with foil normal at 45° to beam.

rich matrix, and (c) comprise irregularly distributed α' and β' phases. The average interlamellar spacing of the cells was estimated to be 30 ± 5 nm, and this dimension will be referred to in subsequent sections dealing with the cooling rates experienced by the splat-quenched foils and the solidification behaviour of representative foil areas.

3.2.1.3. Fine grained material: γ' phase. A bright field (BF) transmission electron micrograph of the first type of very fine-grained material is given in Fig. 6a together with the corresponding selected area diffraction pattern (SADP) and a dark field (DF) image taken by tilting the illumination so that a portion of the first ring of diffracted intensity passed through a 20 μm objective aperature. The DF image shows that the γ' grain size is approximately 3 nm. The microdensitometer trace of the SADP (Fig. 6b) is the lower curve shown in Fig. 7. This curve could be satisfactorily indexed in terms of the γ' phase with a lattice parameter of 0.388 ± 0.006 nm, in agreement with the X-ray results.

Tilting the foil gave SADPs containing arcs of intense diffracted intensity with the arcs lying on ellipses (Fig. 6d), indicating that the fine-grained γ' is strongly textured. Moreover, DF images taken in these tilted orientations showed elongated grains. The fine grained γ' therefore arose as

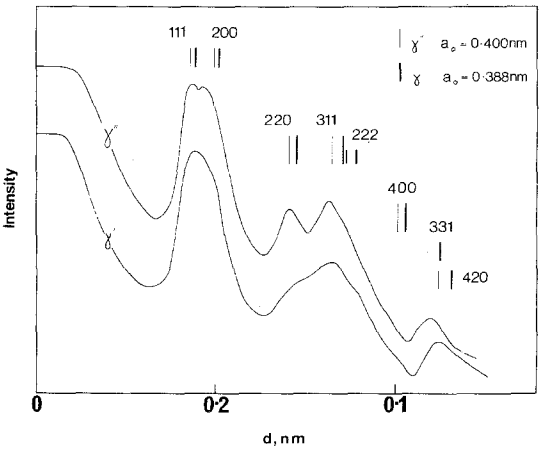

Figure 7 Microdensitometer trace of SADPs of (a) Fig. 6b; γ' phase, and (b) Fig. 8b; γ'' structure.

columnar grains with preferred growth directions normal to the foil surfaces.

3.2.1.4. Fine-grained material: γ'' phase. A BF, DF, SADP set given by the second type of fine-grained material is reproduced in Fig. 8 and a microdensitometer trace of the SADP is the upper curve plotted in Fig. 7. The SADP could not be indexed exactly in terms of any of the lattice parameters for the various fcc phases that were detected by X-ray diffractometry (see Table I) or have been reported to arise in splat-cooled and vapour-quenched foils (6). Equally unsuccessful were attempts to index the pattern by assuming (a) that {2 0 0}, {2 2 0} and {1 1 1} texturing, or combinations thereof, were present, and (b) that the polycrystalline ring pattern was based on numerous, overlapping single-crystal γ' patterns characterized, as has been shown above, by sidebands disposed symmetrically around matrix reflections. Nevertheless, an indexing in terms of the γ'' phase ($a_0 = 0.400$ nm) was the most satisfactory and Fig. 7 gives vertical lines at positions corresponding to the calculated diffraction angles of the various reflections for this phase. However, it must be emphasized that the proposed indexing only represents an approximate, but convenient, description of the second type of fine-grained structure because the observed positions of all the peaks of the microdensitometer trace are not equal to the calculated positions of the appropriate γ'' reflections.

The micromorphology of the very fine-grained γ'' structure was markedly different to that for the fine-grained γ' phase. In particular, DF images showed the γ'' grains to be extended in the plane of the foil while weak intensity variations in SADPs indicated that the elongation direction was parallel to a preferred ⟨1 0 0⟩ γ'' growth direction. The γ'' phase therefore arose as columnar grains lying in the plane of the foil, rather than extending normal to it as was observed to be the case for the γ' phase. Since the preferred columnar growth direction is generally parallel to the predominant heat flow direction, this difference implies that heat removal normal and parallel to the foil surface gave rise to the γ' and γ'' micromorphologies respectively. The significance of this observation in relation to the structure and origin of the γ'' material will be expanded upon in Section 4.3.

3.2.2. Foils aged at room temperature

Extended room-temperature ageing of the partially decomposed γ' phase gave gradual increases in the striation spacing and contrast, and accompanying decreases of the radial sideband separation and tangential sideband intensity. For example, the two-beam image of Fig. 9 ([1 0 0] zone axis, $\mathbf{g} = (0\,0\,2)$), taken after an ageing time of three weeks, shows clearly resolved stirations in BF. The average striation spacing was 7.0 ± 1.5 nm, in agreement with λ_{calc} value of 7.6 ± 1.0 nm calculated from

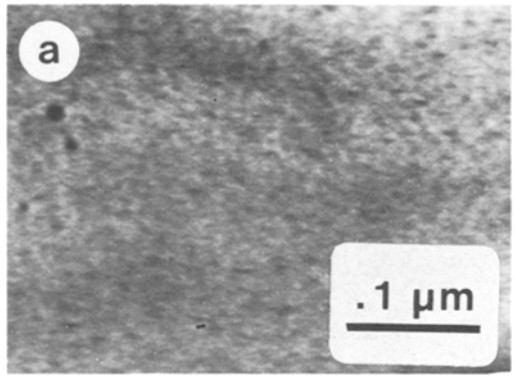

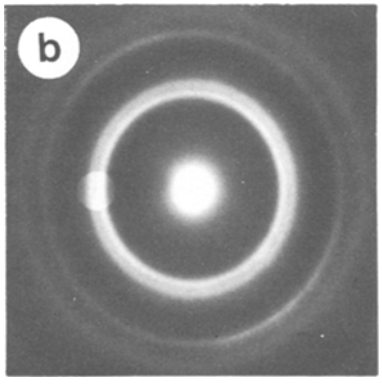

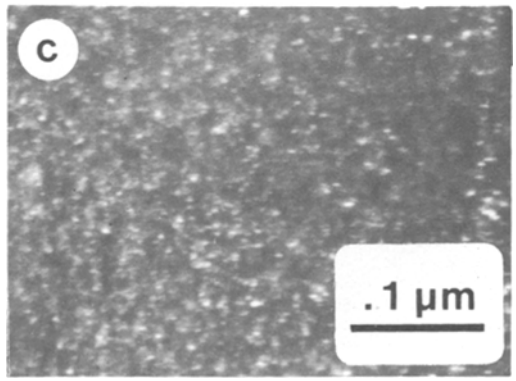

Figure 8 Fine-grained material; γ'' structure: (a) BF micrograph, (b) SADP, (c) DF micrograph, all with foil normal parallel to beam.

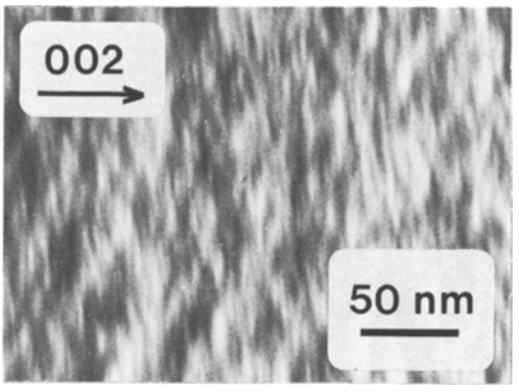

Figure 9 Coarsened spinodal structure obtained by ageing the as-quenched, partially decomposed γ' phase at room temperature for 3 weeks: BF image; [1 0 0] zone axis, g = (0 0 2).

the sideband separation of the corresponding SADP. It therefore appears that the as-quenched γ' structure has coarsened to give more widely separated modulations with a smaller range of orientations.

Further ageing led to the development of large regions of diffuse diffracted intensity. In particular, {2 0 0} reciprocal lattice sections revealed unusually-shaped crosses at matrix reflections, as for example in the SADP of Fig. 10a obtained after three months ageing at room temperature. The enlargement of a {2 0 0} reflections (Fig. 10b) shows that the crosses at {2 0 0} reflections are composed of diffuse streaks in ⟨1 1 0⟩ directions and triangular shaped intensity regions extended in ⟨1 0 0⟩ directions: the streaks are centred on points lying on the low diffraction angle sides of the triangular shaped regions. The SADP can be indexed in terms of coherent Cu-rich zones in a tetragonally distorted Ag-rich matrix. The plate-like zones lie on {2 0 0} matrix planes and give rise to lattice distortions that are manifested by strain-diffuse rel-rods in ⟨1 1 0⟩ directions. Two-beam micrographs taken at this stage, as for example, the BF image of Fig. 10c corresponding to a ⟨1 1 0⟩ orientation with **g** = (0 2 2), revealed contrast striations along the traces of {1 1 0} planes. In all cases, these "basket-weave" striations behaved as if there were lattice displacement vectors in ⟨1 1 0⟩ directions, parallel to the ⟨1 1 0⟩ strain-diffuse rel-rods. Hence extended room-temperature ageing changed the direction of lattice displacement from $\langle 1\,0\,0\rangle_{\gamma'}$ to $\langle 1\,1\,0\rangle_{\gamma'}$.

The BF image of Fig. 11 was obtained after ageing for four months and it can be seen that light-contrasting Cu-rich particles had formed in a dark-contrasting Ag-rich matrix. The accompanying SADP could be satisfactorily indexed in terms of the α (Ag-rich) and β (Cu-rich) terminal solid solutions with $(0\,0\,2)_\alpha \parallel (0\,0\,2)_\beta$ planes approximately normal to the beam direction and $[1\,0\,0]_\alpha \parallel [1\,0\,0]_\beta$. The BF micrograph showed a tendency toward alignment of the β particles in $\langle 1\,0\,0\rangle_\alpha$ directions and the separation between the rows of particles was 7.5 ± 1.0 nm.

It is relevant to note that Stoering and Conrad [4] argued from their bright-field electron metallographic observations of dark-contrasting regions

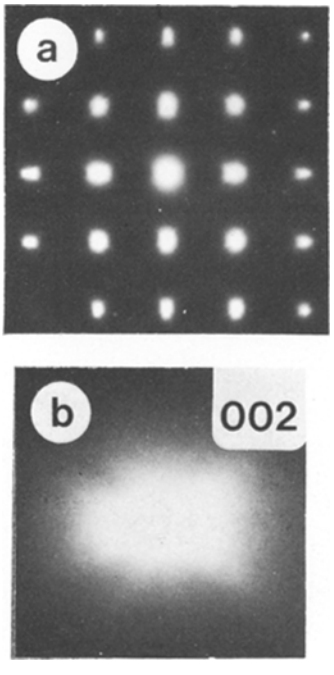

Figure 10 Tetragonally distorted structure obtained after 3 months' ageing at room temperature; (a) SADP, [1 0 0] zone axis, (b) enlargement of the (0 0 2) reflection, (c) BF image (**g** = (0 2 2), zone axis near [1 1 0], shows contrast striations parallel to {1 1 0} traces.

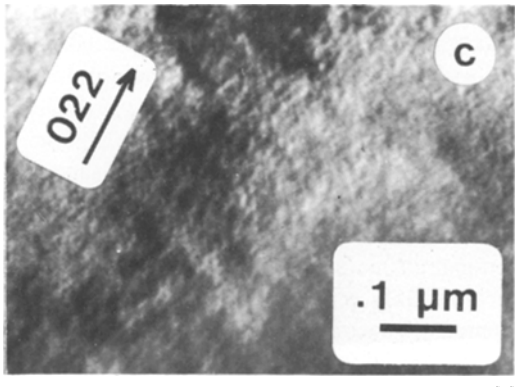

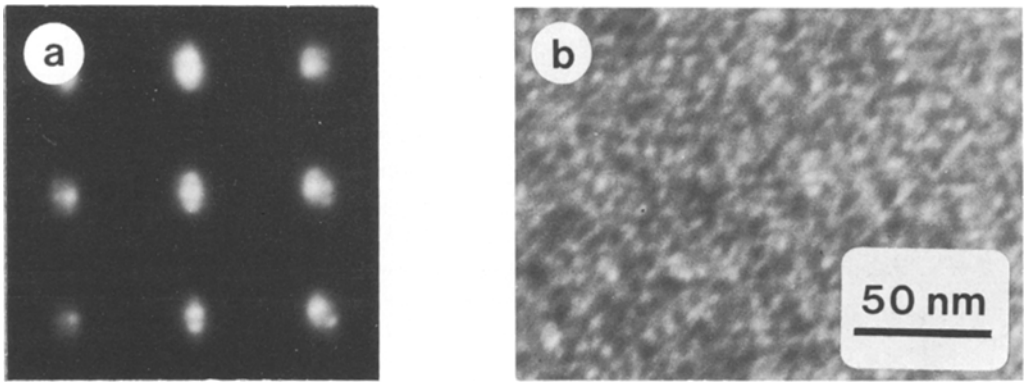

Figure 11 Equilibrium β phase particles in an α matrix obtained after 4 months' ageing at room temperature; (a) SADP, [1 0 0] zone axis; (b) BF image showing particle alignment.

in a light-contrasting matrix of γ' that Ag, rather than Cu, clustering occurred during the decomposition of large γ' grains. However, as was discussed above, epitaxial oxide layers on the surfaces of γ' grains were observed in the present investigation. These layers probably formed during splat-cooling, even though quenching was conducted in a vacuum with a graphite susceptor that gettered oxygen. Since Stoering and Conrad employed considerably more oxidizing splat-cooling conditions, it is likely that their foils were heavily contaminated. As a result, they probably misinterpreted contrast effects due to the oxide as originating from Ag-rich clusters. This being the case, it may be necessary to reconsider many of their conclusions drawn from correlating X-ray and electron metallographic results. A complete re-examination of Stoering and Conrad's results lay outside the scope of this investigation.

In summary, the electron metallographic observations obtained in the present study showed that the extended ageing of the as-quenched modulated structure gave morphological changes similar to those observed in other systems [16] during the coarsening and subsequent equilibration of structures which most likely arose via spinodal decomposition. These changes involved the slow devleopment of a tetragonally distorted structure followed by the rapid formation of spherical β-phase particles, with dimensions that were of the same order of magnitude as the original compositional modulations. The observed structural and transformational characteristics of the striated γ' phase are therefore fully consistent with those expected for a spinodally decomposed structure.

4. General discussion

4.1. The Metastable Ag–Cu Phase Diagram

Silver–copper alloys form a simple eutectic system between Ag-rich α, and Cu-rich β fcc solid solutions and the equilibrium phase diagram (Fig. 12) given by Hansen [17] is well established. Since the atomic radii of Ag and Cu atoms differ by only 12%, and the α and β phases are both face centred cubic, it is reasonable to assume that the solid free energy curve is continuous, though "humped" at large solute concentrations over a temperature range extending from the eutectic temperature T_E to absolute zero [7, 18]. In this event, there will be a metastable, solid state, miscibility gap which has been constructed on the equilibrium phase

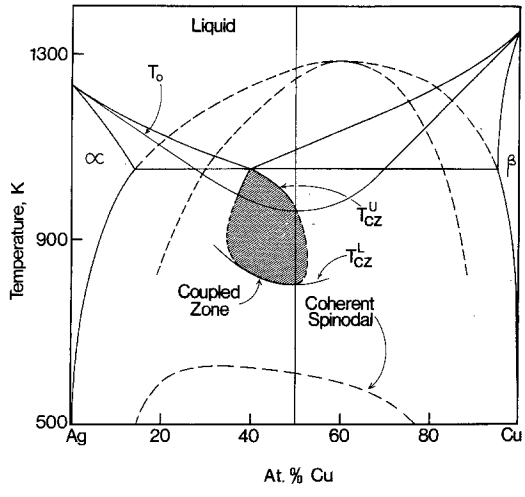

Figure 12 Ag–Cu phase diagram with extrapolated miscibility gap, spinodal curves, T_o lines for massive solidification and coupled zone for co-operative eutectic growth.

diagram of Fig. 12 by extending the $\alpha/\alpha+\beta$ and $\beta/\alpha+\beta$ solvi. The chemical spinodal given in the diagram was then calculated using an expression developed by Cook and Hilliard [19] namely:

$$C_s = C_c + (C_e - C_c)[1 + 0.422T/T_c]$$

where C_s and C_e are the compositions of the chemical spinodal and the miscibility gap limits at a temperature T, while T_c and C_c are the temperature and composition of the critical point. The compositions of the chemical spinodal at T_E, which were obtained from this application of the Cook–Hilliard relation to graphical extrapolations of the equilibrium solvi, agree well (to within ± 5 at.%) with the compositions determined from Sundquist's [18] calculated curve for the free energy of the γ' solid solution at T_E. Finally, the equations and parameters detailed in the Appendix were used to estimated the coherent spinodal curve.

The minimum supercooling, below the equilibrium melting point, required for the solidification of the γ' phase is given by the T_0 line [7]. This line is the locus of points defining the temperature at which solid and liquid of a given composition have the same free energy, and it represents an upper limit of the temperature for the "massive", composition-invarient solidification of γ'. The T_0 curve given in Fig. 12 was plotted as follows: the compositions of the curve at the eutectic temperature T_E were estimated by superimposing Sundquist's calculated solid free-energy curve and a liquid free-energy curve. The latter was obtained by displacing the experimental free-energy curve [18, 20] so that the common-tangent construction gave the equilibrium eutectic composition (39.9 at. % Cu). The intersections of the solid and liquid free-energy curves gave the compositions of the two alloys with the same free energies in both the liquid and solid states. Finally, straight lines through the points corresponding to these compositions, and through the points defining the melting points of the pure components, were extrapolated below T_E in the manner shown in the phase diagram (Fig. 12).

The conditions required for the growth of the second solidification product described in this communication, namely the eutectic cells, are given, phenomenologically, by the coupled zone [21]. This zone defines the temperatures at which alloys of various compositions can solidify by the co-operative growth of the terminal α and β phases. Fig. 12 includes two Ag–Cu coupled zone boundaries between T_E (1058 K) and 980 K that have been determined by Jones *et al.* [22]. Structures comprising massively solidified γ' grains, without coexisting eutectic cells, were often found throughout large volumes of the splat-cooled foils examined in this investigation. This result indicates that it is realistic to suppose there to be a third coupled zone boundary, defining temperatures below which alloys of various compositions form insignificant amounts of the eutectic solidification product. The two experimentally determined boundaries will therefore be referred to as "upper" coupled zone boundaries T_{CZ}^{U}. These boundaries probably tend to converge at high undercoolings due to kinetic effects [23] and they will merge into the third, or 'lower' boundary T_{CZ}^{L} as is shown in Fig. 12.

The lower coupled zone boundary plotted in this figure was calculated by applying classical nucleation and growth theories. Uhlmann [24] has summarized the equations that can be derived, using these theories, for the nucleation and growth rates of a solid phase in an undercooled liquid phase. These equations can be used to calculate the time required for the solidification of a selected, but small (< 10%), volume fraction of solid if it is assumed that the liquid cooled instantaneously to a particular solidification temperature and thereafter crystallized by the isothermal nucleation and growth of solid. In the case of splat-cooled Ag–Cu alloys, since the examination of micrographs containing images of co-existing massive and eutectic solidification products showed that these products appeared to have nucleated independently, it was further assumed that there were two independent solidification reactions involving the crystallization of eutectic cells and of massive γ' grains. Time–temperature–transformation curves were calculated for the solidification of 1 vol% of the two products and these "start" curves are shown in Fig. 13 for the Ag–50 at.% Cu alloy. The equations and the values of the material parameters used in calculating these T–T–T curves are detailed in the Appendix.* A reasonable, but arbitrarily drawn, estimate of the completion or "finish" curve for the massive reaction has also been plotted and a comparison of the eutectic "start" and massive

*Note that the transformation curve labelled "eutectic" was derived assuming *homogeneous nucleation* whereas the coupled zone relates to the *co-operative growth region* and is not specific about nucleation.

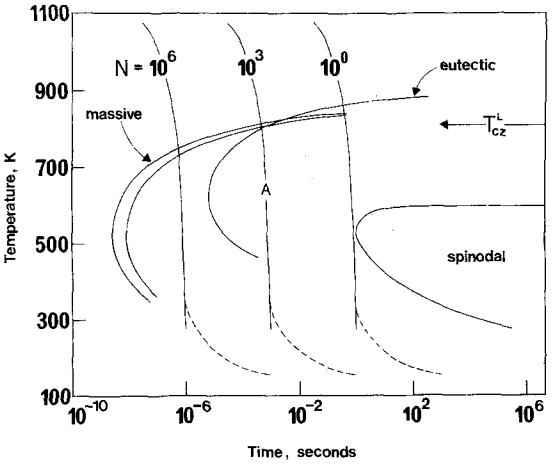

Figure 13 Time–temperature–transformation diagram for an Ag–50 at.% Cu alloy: superimposed continuous lines are cooling curves for Newtonian conditions with indicated values of $N = h/\rho cd$; likely departures from calculated cooling behaviours for constant foil thickness d are indicated by dashed lines. Calculated spinodal "start" curve assumes retention of the melting-point vacancy concentration.

"finish" curves demonstrates that less than about 1 vol% of the eutectic product is predicted to form upon complete solidification at 800 K. This temperature represents an estimate of the temperature T^{L}_{CZ} of the lower coupled zone boundary for the equiatomic alloy and similar considerations for other alloys gave the complete lower boundary given in Fig. 12. It should be noted that T^{L}_{CZ} is weakly dependent on the eutectic volume fraction taken to correspond to the limit of the coupled zone so there is only a small error in T^{L}_{CZ} on assuming the fraction of eutectic cells to be 1%, rather than say 0.01%. Besides, larger errors are introduced by the approximations made in calculating the nucleation and growth rates, and by the assumption that solidification under splat-quenching conditions occurred isothermally instead of during continuous cooling.

4.2. The spinodal decomposition of the γ' phase

Fig. 13 also gives time–temperature–transformation curve for the "start" of the spinodal decomposition of γ', calculated using expressions developed by Cahn [25] and Hilliard [26]. Details of the calculation are summarized in the Appendix. The most important assumption invoked in applying Cahn's linear theory of spinodal transformation, related to the vacancy concentration at the ageing temperature. In particular, there was assumed to be retention, at the transformation temperature, of the vacancy concentration at the equilibrium melting temperature T_m. This is a realistic assumption because it can be shown that the vacancy diffusion distance in the γ' phase during splat-quenching is typically less than 5% of the thickness of the grains examined by electronmicroscopy under two-beam imaging conditions. Hence γ' grains that were observed to have spinodal transformed probably contained a large non-equilibrium vacancy concentration which served to accelerate the transformation.

Ruhl [27] has shown that the cooling rate T from the solidification temperature T_m to T', where T' is the temperature given by $(T' - T_S)/(T_m - T_a) \simeq 0.25$ for a substrate temperature T_a, are well described by the equation

$$\dot{T} = \frac{h}{\rho cd}(T - T_a). \qquad (2)$$

This equation can be derived by assuming that Newtonian cooling conditions prevail during the quenching of a foil of thickness d, specific heat c, density ρ, and heat-transfer coefficient h, at the foil–substrate interface with heat flow normal to that interface. Below T', Ruhl's [27] calculated cooling rates with decreasing temperatures became increasingly smaller than the rates given by Equation 2. Newtonian cooling curves for various values of $N = h/\rho cd$, are superimposed upon the transformation diagram of Fig. 13, together with arbitrarily drawn, but reasonable, curves describing the decreasing cooling rates predicted for temperatures below T'. This figure now demonstrates that N values greater than 1 sec^{-1} ($\dot{T} < 10$ K sec^{-1} from Equation 2) are required for spinodal decomposition to occur during continuous cooling. The same conclusion can be reached by calculating directly the critical cooling rate below which a reasonable amount of spinodal decomposition takes place during the quench [28].

Moreover, reference to Fig. 13 shows that cooling rates large enough to form single phase γ' structures (i.e. structures which do not contain the other experimentally observed solidification product, namely the eutectic cells) would not lead to a significant amount of spinodal decomposition during continuous cooling. For example, if $N > 10^3$ sec^{-1} (Curve A in Fig. 13) then it is predicted that an insignificant amount (less than 1 vol%) of the eutectic product would be formed during

splat-cooling. This value of N corresponds (from Equation 2) to a critical cooling rate $\dot{T}_c = 10^3 \times (820 - 150) = 7 \times 10^5\ \mathrm{K\,sec^{-1}}$ at the solidification temperature (820 K), or a rate of $10^3 \times (610 - 150) = 5 \times 10^5\ \mathrm{K\,sec^{-1}}$ at the coherent spinodal temperature. The latter rate is two to three orders of magnitude greater than the maximum calculated cooling rate ($10^3\ \mathrm{K\,sec^{-1}}$) for the spinodal decomposition of γ' during continuous cooling and is in apparent disagreement with the observation that single-phase γ' structures (i.e. structures containing no eutectic cells) had spinodally decomposed.

In analysing the origin of this discrepancy between the experimental conditions that give rise to spinodally decomposed γ' and the calculated cooling rates for spinodal decomposition during continuous cooling, it is first necessary to examine the accuracies of the calculated transformation curves and the cooling curves. In this context, we note that Cline and Lee [29] have shown experimentally that $S^2G = 1.4 \times 10^{-17}\ \mathrm{m^3\,sec^{-1}}$ for cooperative growth (at a rate G and interlamellar spacing S) of the terminal α and β phases in an eutectic Ag–39.9 at.% Cu alloy. Hence the average interlamellar spacing of the eutectic cells observed in this investigation (Fig. 5) corresponds to a growth rate of $0.016\ \mathrm{m\,sec^{-1}}$ at their solidification temperature (800 K from Fig. 13). Assuming Newtonian cooling conditions, the cooling rates $\dot{T}_E$ required to establish this eutectic growth is GL'/cd, where L' is the latent heat per unit mass for eutectic solidification and d is the effective foil thickness, or equivalently, the length of the heat transfer path. For $L' = 200\ \mathrm{J\,g^{-1}}$ and $c = 0.385\ \mathrm{J\,g^{-1}}$, we have $\dot{T}_E \simeq 8/d\ \mathrm{K\,sec^{-1}}$. The γ' grains surrounding the eutectic cells shown in Fig. 5 were elongated in a direction normal to the boundaries between the electron-transparent area and the surrounding opaque material, indicating that heat flow took place in the plane of the foil. The half-width of the thin region was $\simeq 5\ \mu\mathrm{m}$ and if it is assumed that this distance is equal to d, then $\dot{T}_E \simeq 10^6\ \mathrm{K\,sec^{-1}}$. This rate is in good agreement with the critical cooling rate $\dot{T}_c = 7 \times 10^5\ \mathrm{K\,sec^{-1}}$ (calculated from Equation 2 and the transformation curves of Fig. 13) less than which the simultaneous solidification of γ' and the eutectic product could occur. The high temperature segments of the cooling curves plotted in Fig. 13 are therefore representative of the cooling conditions experienced by the foils. However, the cooling rates at lower temperatures may diverge more drastically from values predicted by Equation 2 than has been indicated in Fig. 13 by the dashed lines. These lines were drawn assuming a constant d but it is likely that the effective length of the heat transfer path increased during splat-cooling in the solid state due to foil detachment from the substrate brought about by contraction of the foil. Nevertheless, this length is unlikely to increase by the several orders of magnitude required for the critical cooling curve for single phase γ' solidification (Curve A in Fig. 13) to intersect the nose of the spinodal C curve. It is therefore concluded that spinodal decomposition did not take place during splat cooling but during room-temperature ageing prior to electron metallographic examination of the splat-cooled foils.

In support of this conclusion are the observations that (a) the modulation wavelengths, λ_{calc} and λ_{exp} were constant in different foils aged for the same time; (b) the smallest λ_{exp} that could be resolved (5.5 ± 1.5 nm) was equal to the theoretically predicted value, λ_{calc} of 5 ± 1 nm; and (c) the calculated room-temperature transformation time (2×10^4 sec, accurate to within plus or minus one order of magnitude giving $2 \times 10^3 - 2 \times 10^5$ sec) is not significantly different to the actual room-temperature ageing time (2×10^3 sec) required for the detection of resolvable sidebands. Cahn's [25] linear theory of spinodal decomposition therefore describes the transformation characteristics if the decomposition of the γ' phase took place during ageing at room temperature.

4.3. The γ' grain size

The proposed solidification model, based upon Uhlmann's analysis [24], also accounts for the presence, in splat-quenched Ag–50 at.% Cu foils, of γ' with a wide range of grain sizes (3 nm to 1 μm). Briefly, the model can be used in conjunction with the theory of transformation kinetics to calculate the completion time for solidification of γ' at a particular temperature. This completion time, together with Uhlmann's expressions for the homogeneous nucleation rate and the massive growth of γ' (see the Appendix) are then combined to give the average grain size following massive solidification of the alloy at the specified temperature. This calculated grain size, for isothermal transformation, also represents a reasonably accurate estimate of the grain size produced by continuously cooling the melt along

a cooling curve that intersects the massive solidification "start" curve (Fig. 13) at the specified temperature. Further details of this procedure for calculating the massive grain size in splat-quenched foils will be presented elsewhere. However, preliminary results for a Ag–50 at.% Cu alloy predict that the γ' grain size is 0.5 μm after cooling under Newtonian conditions with $N = 10^3$ sec^{-1} ($\dot{T} = 7 \times 10^5$ K sec^{-1}, Curve A in Fig. 13); and 3 nm on cooling with $N = 10^8$ sec^{-1} ($\dot{T} = 5 \times 10^{10}$ K sec^{-1}). The former value of the grain size is approximately equal to that observed in areas containing γ' and a small volume fraction of the eutectic product (Fig. 5), i.e. in areas that experienced a thermal history given by Curve A. Secondly, it is predicted that the observed grain-size range (3 nm to 1 μm) is produced by a five fold change in h/d (h/d $\propto$ N, Equation 2). Variations of this order of magnitude within a single foil are thought to arise in electron-transparent areas of splat-quenched alloys [7]. Hence the proposed soldification model, based upon homogeneous nucleation and massive growth, accounts for and predicts satisfactorily the wide range of observed γ' grain sizes.

Evidence for columnar growth of the γ' phase normal to the foil surfaces was obtained in this investigation, suggesting that surface nucleation, rather than homogeneous nucleation, took place. However, it can be shown that for a given high cooling rate, the average size normal to the columnar growth direction of surface-nucleated grains is approximately equal to the average size, in all directions, of homogeneously nucleated grains. Hence, the solidification model can be extended to provide reasonably accurate estimates of the grain sizes in surface nucleated structures. The significance of this result will be demonstrated in the next section dealing with the fine-grained γ'' material.

4.4. Lateral heat flow splat-cooling: a possible origin of the fine-grained γ'' structure

The cooling rate calculations presented were shown to be consistent with the observed interlamellar spacing of the eutectic nodules if lateral heat flow had taken place during solidification. The frequent observations of large elongated γ' grains, both separate from, and in conjunction with, the nodules support this conclusion. Similarly, it will be shown below that while the origin of the remaining structure described above, namely the fine-grained γ'' material, could not be rationalised directly in terms of the solidification model presented in Section 4.1, it is possible to argue that some of the fine-grained γ' areas decomposed to the γ'' structure during splat-cooling under lateral heat-flow conditions. It should however, be noted that although there was no evidence for the transformation of γ' to γ'' on ageing at room temperature, the possibility of this transformation sequence at higher temperatures during splat-quenching cannot be discounted.

Proceeding accordingly, we observe that if the γ'' material is assumed to be partially decomposed γ', then it is only necessary to consider the solidification of γ'. The proposed solidification model discussed above, predicts that the formation of γ' with a given grain size only requires a particular cooling rate to be established during solidification. The fine-grained γ' and γ'' (partially decomposed γ') have similar grain sizes, in the columnar growth directions, so they solidified at approximately the same cooling rate. However, the fine-grained γ' material arose as small columnar grains orientated normal to the splat-cooled foil surfaces, in contrast to the γ'' structure which comprised columnar grains of a similar size lying in the plane of the foil. Maintaining the proposal that γ' transformed to γ'', these morphological characteristics imply that the γ' phase, with a small grain size, grew during solidification in directions both normal and parallel to the foil-substrate interface as a result of vertical and lateral heat flow. In the case of vertical heat flow, $d \simeq = 0.1\,\mu$m (the true foil thickness of an electron-transparent area) while for lateral heat flow $d \simeq 5\,\mu$m (the average half-width of a typical fine grained γ'' area). Jones [7] has pointed out that cooling will be Newtonian ($\dot{T} \propto d$) for $d \simeq 0.1\,\mu$m and $h = 10^5$ W m^{-2} K^{-1}, the latter being the average of several experimentally determined values of the heat transfer coefficient for splat-cooling. On the other hand, to attain the same cooling rate ($\simeq 10^8$ K sec^{-1}) with $d = 5\,\mu$m, it is necessary for h to be 10^7 W m^{-2} K^{-1} and consequently, "intermediate" cooling conditions, with $T \propto d^{-x}$ where $x \simeq 1.5$, will be established [7]. In other words, for a given grain size, the cooling rates of those areas experiencing lateral heat flow are more dependent on d than those experiencing normal heat flow. Thus any increase in d, due to the foil detachment effect referred to above, would lead to more severely reduced solid-state cooling rates in the case of lateral heat

transfer. Hence the observation of laterally solidified γ'' grain structures does not conflict with the proposal that the γ'' material formed as a result of the solid-state decomposition of the fine-grained γ' phase.

5. Conclusions

(1) X-ray diffractometry indicated that foils of a splat-cooled Ag–50 at.% Cu alloy, prepared by quenching in a vacuum on to a cold (150 K) substrate, were predominately composed of the γ' phase, an extended solid solution with a lattice parameter of 0.3878 nm, corresponding to a + 1% deviation from the Vegard line.

(2) Immediate examination of electron-transparent areas of the as-quenched foils by transmission electron microscopy revealed that the γ' phase possessed grain sizes ranging from $\simeq 3$ nm to 2 μm.

(3) The coarse grained γ' phase was shown by transmission electron microscopy to have microstructural and transformational characteristics similar to those expected of a spinodally decomposed structure.

(4) Since suppression of the spinodal decomposition of γ' was not observed, the X-ray results, which were identical to those previously reported by other workers and which imply that untransformed γ' in splat-cooled Ag–50 at.% Cu alloys can be retained at room temperature, are misleading.

(5) Calculation of the theoretically predicted "start" times for the spinodal decomposition of γ' indicated that the solid-state reaction took place during ageing at room temperature, prior to electron metallographic examination of the thin foils, rather than during the quench.

(6) A model for the solidification of rapidly cooled eutectic alloys was developed and applied to the Ag–Cu system. The model satisfactorily described the overall microstructural features of the splat-quenched foils.

6. Appendix

6.1. Coherent spinodal

Following Cahn [25] and Hilliard [26], the temperature of the coherent spinodal T_s^* assuming ideal entropy of mixing is given by

$$T_s^* = T_s - 2\eta^2 Y N_v k / C_0(1 - C_0)$$

where T_s is the temperature of the chemical spinodal for an alloy composition c_0; the elastic constant function Y, is equal to $C_{11} + C_{12} - 2(C_{12}^2/C_{11})$ for modulations on {2 0 0} planes in cubic crystals with $2C_{44} - C_{11} + C_{12} > 0$; $\eta = -(d \ln a_0/dc)_{c_0}$ where a_0 is the lattice parameter; N_v is the number of atoms per unit volume; k is Boltzmann's constant; and C_{ij} are the elastic constants.

The elastic constants of an Ag–50 at.% Cu alloy were taken to be the averages of the temperature dependent constants for pure Ag and pure Cu [30]; the value of η for the same alloy was calculated from a fourth-order polynomial fitted to the reported lattice parameters for γ' phases of various compositions [1, 2, 6, 9].

6.2. Time–temperature–transformation curve for spinodal decomposition

The "start" time for spinodal decomposition was assumed to be the reciprocal of R_m, the amplification factor of the Fourier component of the wavelength λ_m, receiving maximum amplification [25]. For an ideal entropy of mixing,

$$R_m = (T - T_s^*)^2 N_v k^2 M / 8K c_0^2 (1 - c_0)^2,$$

where the atom mobility M, is such that,

$$M = [c_0(1 - c_0)/kT] \times [D_0 \exp(-E/kT) \exp(-E^*/kT_q)]$$

The constant D_0 was assumed to equal the average of the pre-exponential constants for Ag tracer diffusion in Cu and Cu tracer diffusion in Ag (i.e. $D_0 = 0.93$). Assuming retention, at an ageing temperature T, of the vacancy concentration at $T_q = T_m$, we have $E = E_m$ and $E^* = E_f$. The activation energies for vacancy formation E_f and migration E_m were taken to be 99.6 and 78.1 kJ mol^{-1} [31]. The gradient energy coefficient, K, was assumed to equal $N_v k T_s \psi^2 / 4c_0(1 - c_0) = 11 N_v k T_s a_0^2 / 56 c_0 (1 - c_0)$ for an interaction distance ψ, given by a Leonard–Jones 6/12 potential.

The assumptions presented above also predict [25, 26]

$$\lambda_m^2 = 88\pi^2 T_s a_0^2 / 7(T - T_s^*)$$

6.3. Time–temperature–transformation curves for massive and eutectic solidification

Following Uhlmann [24], the time for the formation of a volume fraction X at a temperature T, is approximately $(3X/I_v G^3)^{1/2}$ where the nucleation rate per unit volume $I_v = N_v kT \exp[-PT_m^5/(T_m - T)^2 T^3]/3\pi\mu^3\eta$. For massive solidi-

fication, $P = 1.024$, and the growth rate, $G = \beta kT[1 - \exp(-L\Delta T/RT_0T)]/3\pi a_0\mu\eta$ [24, 32]. R, β, μ and η are the gas constant, a geometric constant, the correlation length for liquid diffusion and the liquid viscosity respectively; L is the latent heat per mole for massive solidification; T_m is the equilibrium melting point; T_0 has been defined in the text and $\Delta T = T - T_0$. For eutectic solidification, $p \simeq 2$ and $G = W\eta_E(T - T_E)^2T/4\phi^2\eta T_E$ where $W = S^2G$ and $\phi = 2\sigma_{\alpha\beta}T_E/L'$ [31]: η_E is the viscosity at T_E, the eutectic temperature; S is the interlamellar spacing; L' is the latent heat per mole for eutectic solidification of the α and β phases and $\sigma_{\alpha\beta}$ is the interphase boundary energy.

The following values of the parameters appearing in the above expressions were used in calculating the T–T–T curves:

$$a_0 = 0.3876\,\text{nm}, \quad \mu = 2a_0,$$

$$N_v = 6.2 \times 10^{28}\ \text{atoms m}^{-3}$$

$$\beta = 10, \quad W = 14. \times 10^{-17}\ \text{m}^3\ \text{sec}^{-1}\ [27],$$

$$\sigma_{\alpha\beta} = 0.2\,\text{J m}^{-2}$$

$$L = L' = 200\,\text{J g}^{-1}$$

$$\eta = C\exp(-Q/RT)$$

where $Q = 20.0\,\text{kJ mol}^{-1}$, $C = 0.56\,\text{mPa sec}$ these values Q and C being the averages of Arrhenius equation constants for the viscosities of pure Ag and pure Cu.

Acknowledgements

The authors are indebted to the Australian Research Grants Committee for supporting this research.

References

1. P. DUWEZ, R. H. WILLENS and W. KLEMENT JR., *J. Appl. Phys.* **31** (1960) 1136.
2. R. K. LINDE, *ibid* **37** (1966) 934.
3. M. C. FLEMINGS, "Solidification Processing" (McGraw-Hill, New York, 1974) p. 278.
4. R. STOERING and H. CONRAD, *Acta Met.* **17** (1969) 933.
5. S. NAGAKURA, S. TOYAMA and S. OKETANI, *ibid* **14** (1966) 73.
6. B. PREDEL and G. SCHLUCKEBIER, *Z. Metallk.* **63** (1972) 782.
7. H. JONES, *Rep. Prog. Phys.* **36** (1973) 1425.
8. P. DUWEZ and R. H. WILLENS, *Trans. Met. Soc. AIME* **227** (1963) 1581.
9. T. B. MASSALSKI, Z. F. VASSAMILLET and Y. BIENVENU, *Acta Met.* **21** (1973) 649.
10. J. V. WOOD and R. W. K. HONEYCOMBE, *J. Mater. Sci.* **9** (1974) 1183.
11. J. V. CATHCART and G. F. PETERSEN, *J. Electrochem. Soc.* **115** (1968) 595.
12. M. BOUCHARD and C. THOMAS, *Acta Met.* **23** (1975) 1485.
13. J. W. CAHN, *Acta Met.* **14** (1966) 1685.
14. V. DANIEL and H. LIPSON, *Proc. Roy. Soc. A.* **181** (1943) 368.
15. E. P. BUTLER, *Met. Sci. J.* **5** (1971) 8.
16. E. P. BUTLER and G. THOMAS, *Acta Met.* **18** (1970) 347.
17. M. HANSEN, "Constitution of Binary Alloys", (McGraw-Hill, New York, 1958) p. 18.
18. B. E. SUNDQUIST, *Trans. Met. Soc. AIME* **236** (1966) 1111.
19. H. E. COOK and J. E. HILLIARD, *ibid* **233** (1967) 142.
20. R. HULTGREN, P. D. DESAI, D. T. HAWKINS' M. GLEISER and K. K. KELLEY, "Selected Values of the Thermodynamic Properties of Binary Alloys", ASM, Ohio, 1973) p. 44.
21. A. KOFLER, *Z. Metallk.* **41** (1950) 22.
22. B. L. JONES, G. M. WESTON and R. T. SOUTHIN, *J. Cryst. Growth* **10** (1971) 313.
23. H. FREDRIKSSON, *Met. Trans. A* **6A** (1975) 1658.
24. D. R. UHLMANN, *J. Non-Cryst. Solids* **7** (1972) 337.
25. J. W. CAHN, *Trans. Met. Soc. AIME* **242** (1968) 166.
26. J. E. HILLIARD in "Phase Transformations", (A.S.M., Ohio, 1970) p. 497.
27. R. C. RUHL, *Mater. Sci. Eng.* **1** (1967) 313.
28. E. L. HUSTON, J. W. CAHN and J. E. HILLIARD, *Acta Met.* **14** (1966) 1053.
29. H. E. CLINE and D. LEE, *ibid* **18** (1970) 315.
30. G. SIMMONS and H. WANG, "Single Crystal Elastic Constants and Calculated Aggregate Properties: Handbook", (M.I.T. Press, Cambridge, 1971).
31. R. A. JOHNSON in "Diffusion", (A.S.M., Ohio, 1972) p. 25.
32. J. W. CAHN, W. B. HILLIG and G. W. SEARS, *Acta Met.* **12** (1964) 1421.
33. W. A. TILLER, "Liquid Metals and Solidification", (A.S.M., Ohio, 1958) p. 276.

Received 15 September 1976 and accepted 4 January 1977.